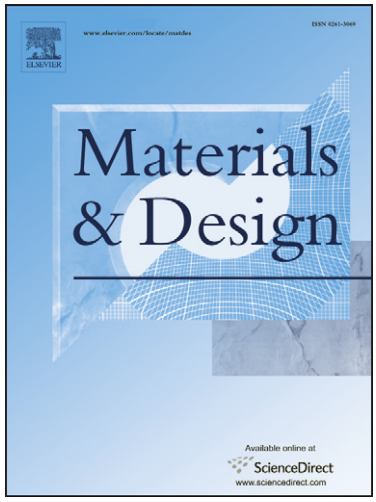

Effect of welding procedure on wear behaviour of a modified martensitic tool steel hardfacing deposit

Agustín Gualco, Hernán G. Svoboda, Estela S. Surian, Luis A. de Vedia

PII: S0261-3069(10)00237-2
DOI: 10.1016/j.matdes.2010.04.026
Reference: JMAD 3077

To appear in: *Materials and Design*

Received Date: 3 November 2009
Accepted Date: 14 April 2010

Please cite this article as: Gualco, A., Svoboda, H.G., Surian, E.S., de Vedia, L.A., Effect of welding procedure on wear behaviour of a modified martensitic tool steel hardfacing deposit, *Materials and Design* (2010), doi: 10.1016/j.matdes.2010.04.026

Effect of welding procedure on wear behaviour of a modified martensitic tool steel hardfacing deposit

Agustín Gualco [(1)*], Hernán G. Svoboda [(2)], Estela S. Surian [(1, 3)], Luis A. de Vedia [(4)]

[(1)] RESEARCH SECRETARIAT, Faculty of Engineering, National University of Lomas de Zamora, Lomas de Zamora, Province of Buenos Aires, Argentina.

[(2)] MATERIALS AND STRUCTURES LABORATORY, Faculty of Engineering, University of Buenos Aires, INTECIN, CONICET, Buenos Aires, Argentina.

[(3)] DEYTEMA, Regional Faculty of San Nicolás, National Technological University, San Nicolás, Province of Buenos Aires, Argentina.

[(4)] INSTITUTE OF TECHNOLOGY PROF. JORGE A. SABATO, National University of San Martín (UNSAM-CNEA), San Martín, Province of Buenos Aires, Argentina.

Abstract

In the last years hardfacing became an issue of intense development related to wear resistant applications. Welding deposits can functionalize surfaces and reclaim components extending their service life. Tool steels are widely used in hardfacing deposits to provide improved wear properties. Nevertheless systematic studies of wear behaviour of new alloys deposited by hardfacing, under different service conditions are scarce. In this work the effects of shielding gas, heat input and post weld heat treatment on the microstructural evolution and wear resistance of a modified AISI H13 martensitic tool steel deposited by semi-automatic gas shielded arc welding process using a tubular metal-cored wire, were studied. Four coupons were welded with different welding parameters. The shielding gases used were Ar-2% CO_2 and Ar-20% CO_2 mixtures and two levels of heat input were selected: 2 and 3 kJ/mm. The as welded and 550ºC-2 hours post weld heat treated conditions were considered. From these coupons, samples were extracted for testing metal-metal wear under condition of pure sliding with a load of 500 N. Chemical compositions were determined; microstructure and microhardness were assessed. It was found that content of retained austenite in the microstructure varied with the welding condition and that heat treated samples showed secondary hardening, associated with precipitation phenomena. Nevertheless, as welded samples showed higher wear resistance than heat treated specimens. Under these test conditions post weld

Corresponding autor. Tel.: +54 11 4282 7880
E-mail: agustingualco@yahoo.com.ar

heat treatment led to a reduction in wear resistance. The best wear behaviour was observed in samples welded with low heat input and under the lowest oxygen potential shielding gas used here, in the as welded condition. The intervening mechanism was mild oxidative. These results were explained in terms of the relative oxidation resistance stemming from different welding conditions.

Key Words: A. Ferrous metals and alloys; E. Wear; D. Welding

1. Introduction

Hardfacing is a widely used method to treat surfaces subjected to severe wear, corrosion or oxidation which has become an important field of application and technological development for the manufacturing of new components, their repair and their service life extension for the most varied industries [1]. In this respect, the systematic study of consumables and welding procedures applied for hardfacing is of interest to optimize the design of consumables and to develop and evaluate welding procedures. Thus, the heat input, the shielding gas, the preheating temperature and the post-weld heat treatment (PWHT) are some of the process variables of relevance that control the microstructural development and hence influence of final properties.

Tubular wires have become one of the most common welding consumable options, because they have both high productivity and flexibility for manufacturing alloy grades, introducing an economic alternative for major productions [2]. The metal-cored tubular wires are consumables with the added advantage of a very low slag generation, lower smoke production and higher deposition rates [3-4]. However there is scarce available information related to systematic studies on this kind of consumables, particularly for hardfacing materials.

In general, hardfacing materials for wear resistance applications can have high hardness in the as welded condition but also achieved through heat treatment or mechanical work. The microstructure may consist of martensite or of a soft matrix with hard particles or second phases (carbides or borides) according to the type of application required [5]. For metal-metal sliding or rolling, where wear is mainly due to sub-surface fatigue, oxidation and adhesion, materials with carbon content between 0.1 and 0.7 wt% and up to 20 wt% alloy (Cr, Mn, Mo, W and/or V) are usually employed [1, 6]. AISI H13 steel (5 wt% Cr with 0.5

wt% C, Mo and V) is a typical martensitic tool steel that is widely used in hot and cold working for engineering applications [7]. The welding deposits often require a PWHT to enhance their wear behaviour. These treatments regulate the resulting mechanical properties and provide stress relieving which can be of great significance for the life of a component [8].

Among the different wear mechanisms, mild oxidative is characterized by the formation of oxide layers on the sliding surfaces between two pieces, which strongly influences wear behaviour. In the initial stage of the sliding process a severe wear occurs and opposed surfaces achieve conformity. An area of actual contact, consisting of several large plateaus, is established. Given sufficient frictional heating the contacting plateau oxidize preferentially. Oxide islands are developed on this surface carrying the external load. Therefore, the plateau grows in height. In the course of many passes this increase in height is spread over the whole contacting area. Beyond a critical oxide film thickness, the plateau becomes unstable and breaks up to form wear debris. Then, other load-bearing plateau elsewhere on the surface becomes operative as areas of clean metallic surface come into rubbing contact and oxidize. The above description cycle starts again and the oxidative wear mechanism advances [9-10]. This wear mechanism could be operative in a range of service conditions, where low loads and slow velocities are characteristic [11].

The objective of this work was to study the effect of welding parameters - heat input, shielding gas type and post weld heat treatment - on wear resistance of hardfacing deposits of a modified tool steel, to contribute to a better understanding of the existing relationship between welding procedure, microstructural evolution and wear resistance of martensitic steel weld deposits produced with metal-cored tubular wire, working in low contact stress conditions.

2. **Experimental Procedure**

2.1. Welded specimens

Four 375x75x19 mm SAE 1010 carbon steel plates were used as base material. On each plate, four layers with 5, 4, 4 and 3 passes per layer were deposited as shown in Figure 1.

Each coupon was welded under different conditions, varying heat input and the type of shielding gas. The welding parameters employed can be seen in Table 1.

The consumable employed was a 1.2 mm diameter metal-cored wire used with a mechanized gas metal arc welding (GMAW) process using an automatic Railtrac FW1000 Flexi Weaver. The stick out was 20 mm and the gas flow rate 20 L/min. The welding position was flat; preheating and interpass temperatures were 150 ºC. The quality of the welded coupons was evaluated by radiographic testing.

Each welded coupon was divided in two: one half was heat treated at 550ºC during 2 hours and the other one was kept in the as welded (AW) condition. Identification: RC, RH, TC, TH are AW samples; RCP, RHP, TCP, THP are PWHT samples, Table 1.

2.2. Weld metal characterization

Transverse cross sections from each coupon were extracted for chemical analysis, microstructural characterization and wear testing. The chemical composition was determined by optical emission spectrometry (OES) on the last pass for each condition; C was analyzed by LECO equipment. The microstructure was characterized by light microscopy (LM), scanning electron microscopy (SEM) and X-ray diffraction (XRD). From XRD patterns, the retained austenite fraction was estimated by means of the direct peak comparison method and the remaining residual stresses by the Williamson-Hall method [12]. An electrolytic dissolution technique was employed to evaluate precipitated particles [13]. The particles extracted were analyzed by means of XRD.

2.3. Wear testing and microhardness measurements

The welded samples were tested for wear resistance in pure sliding, with an AMSLER machine, using an AISI 1020 steel as a reference material. The applied load was 500 N and the sliding velocity during the test 0.46 m/s. The test pieces and the reference wheel had a radius R = 20 mm; their geometry and dimensions (in mm) are shown in Figure 2. The surface roughness for both pieces (plate and wheel) was Ra = 0.8 μm.

The applied load on the surfaces in contact generated a low contact stress. After being tested, the samples were ultrasonically cleaned and weighed in a 0.1 mg accuracy analytical balance. Vickers 1 kg microhardness (HV1) was also measured on a transverse cross section near the wear surface in the numbered locations shown in Figure 3.

The wear behaviour was assessed as a function of the distance travelled during wheel/plate sliding, measuring the weight loss for 275, 550, 825, 1100, 1375, 1650, 3300 and 4950 m; 3 sets (plate-wheel) for each welded condition were tested and average values were calculated.

2.4. Characterization of tested samples

Both plate and wheel worn surfaces were analyzed by LM, SEM and XRD, as well as the transverse cross sections of the tested samples, to study the wear mechanisms involved. The debris produced was collected after each testing interval. These collected particles were also characterized by XRD and SEM. Local chemical composition was assessed using energy dispersive spectrometry (EDS).

3. **Results and Discussion**

3.1. Macrostructure

Figure 4 presents the cross sections of the welded specimens showing the base metal, the hardfacing material and absence of macroscopic defects (pores, slag inclusions, cracks, etc.). This fact was confirmed by X-ray testing where the level of reported defects was low.

As can be seen in Figure 4, samples TH and RH, welded with higher heat input showed higher thickness deposits (25 mm) than TC and RC welded with lower heat input (18 mm). In previous studies on dilution effects conducted with this material [14] it was found that, for these welding conditions, from 13 mm thickness upward, the deposit reached the all-weld metal composition of the consumable. Thus, when working with the highest heat input used in this work one layer could be saved.

3.2. Chemical composition

Table 2 shows the results of the chemical composition measured on the surface of the last pass of each sample.

The deposited material was a modified version of an AISI H13 tool steel with higher contents of Mn and Mo and the addition of 2 wt% of W. These changes in chemical composition were designed to improve the wear behaviour of these deposits.

There was a little effect of shielding gas and heat input on the chemical composition of the hardfacing deposits. When the shielding gas with higher oxygen potential was used (Ar-20%CO_2), there was a higher oxygen concentration in the arc atmosphere, then a larger proportion of deoxidant elements were consumed, so that the weld metal showed a reduced amount of these elements [15-16]. Chemical composition was slightly impoverished in alloying elements in the weld deposits produced under the gas mixture with higher CO_2 content.

Considering the coupons welded under the same shielding gas, there were slightly lower contents of Mn and Si in those samples produced with higher heat input. This fact could be associated with the additional time for welding pool reactions in the high heat input samples regarding to those with lower heat input.

The observed variation in chemical composition could have affected the microstructural evolution due to its effect on phase transformation phenomena.

3.3. Microstructure

Figure 5 shows the microstructures of as welded weld metal deposits. These images were obtained in a cross section at 100 microns below the wear surface, corresponding to the area identified as 1 in Figure 3.

All these samples showed a microstructure composed of martensite and retained austenite, with a pattern of dendritic segregation which became more refined as heat input was reduced. These observations were consistent with what was expected for this type of material [17].

In addition, given the increased alloy content detected in the interdendritic area [14], there was a local decrease in the austenite to martensite transformation start temperature (M_s), so that retained austenite was present in that area [5]. During the welding bead cooling process the precipitation of small carbides of M_3C y $M_{23}C_6$ types was produced [17]. On the other hand, as the deposits were multilayer the microstructure was tempered [18] by subsequent passes, producing further precipitation of these small carbides, which darken martensite. Both effects were maximum for higher heat input and higher CO_2 content in the gas shielding, as previously found by the authors [14].

In all cases, after the PWHT, both decomposition of retained austenite in martensite and precipitation of fine carbides were observed. Figure 6 shows high resolution SEM images of RCP sample in which carbides, microcracks and martensite laths formed from retained austenite could be observed.

Figures 7 shows the XRD pattern of extracted carbides of RCP specimen. It was previously reported that in this material precipitated carbides could be $M_{23}C_6$, M_7C_3, M_2C and MC types [19-20]. As it could be observed, precipitated carbides found in sample RCP were consistent with those reported in literature.

Figures 8 and 9 show XRD patterns for AW and PWHT samples, respectively. Austenite and martensite were detected. The remaining residual stresses estimated in AW samples were in the range of 525 to 595 MPa while in PWHT samples it was of 260 to 330 MPa; these last ones showed a marked stress relieving effect. Heat-treated samples showed a reduction of the austenite peaks intensity, in agreement with the metallographic observations. This phenomenon was associated to the activation of diffusion mechanisms of alloying elements retained in the austenite. As a consequence precipitation of carbides and transformation of austenite to martensite were produced.

Figure 10 shows the retained austenite contents for the different samples, obtained from the analysis performed using the peak comparison method to quantify phases based on the XRD patterns.

RC condition presented the highest content of retained austenite: 16%. This was probably due to the fact that this was the sample richest in alloying elements such as C, Mn, Mo and V, which would result in higher values of retained austenite. The other samples showed about 10% of retained austenite. In PWHT condition retained austenite transformed almost completely into martensite, remaining the same tendency observed for AW conditions.

The chemical composition could be related to M_s temperature using experimental expressions developed for this type of materials [5, 19]. Calculated M_s temperatures were correlated to the percentage of retained austenite measured in the different samples. Figure 11 shows that there was a good correlation among the experimental data.

The relationship between the retained austenite (γ) content and M_s temperature obtained from this analysis is shown in the Eq. (1).

$$\gamma\ [\%] = 39 - 0.168 \times M_s\ [^{\circ}C] \qquad (1)$$

This allows quantification of the fraction of retained austenite from the chemical composition of the weld deposit.

3.4. Microhardness

Figure 12 shows the microhardness values measured near the wear surface, for all the samples. In welds produced with low heat input a decrease in hardness was detected. This could be related to the increased fraction of retained austenite in the RC condition (16%) and to the decrease in carbon content (0.40%) of the martensite for the TC condition [21]. Indeed, less precipitation hardening effect related to reheating in a multilayer deposit could be associated with low heat input welds.

All the PWHT samples showed a secondary hardening effect accompanied by the transformation of retained austenite into martensite which resulted in an increase in hardness when compared to the AW conditions. The RC specimen showed the highest hardness associated with the highest alloying element content and the largest proportion of transformation of austenite into martensite. For the tempering temperature used in this paper, the precipitation hardening effect showed its maximum, as previously found [22].

3.5. Wear behaviour

3.5.1. Wear rate

Figures 13 shows the weight loss results as a function of sliding distance for all conditions analyzed. The reached equilibrium temperature during the test was about 130 °C, measured near the wear surface. Wear rates based on the test results were obtained by a linear regression fit of the weight loss vs. sliding distance curves. Figure 14 presents the values obtained for each condition.

The AW samples showed better wear resistance than PWHT specimens. The reason for this behaviour could be the precipitation of chromium in solution, forming carbides during the heat treatment; thus the metal matrix diminished its chromium content, decreasing the resistance to oxidation of the metal [9, 23]. Taking into account that the predominant wear mechanism was mild oxidative, promoted by the test conditions (low load and low speed), the oxidation resistance of the material would have controlled the wear rate while hardness was not determinant [24]. This superior performance of the AW condition is not usually found [21]. It was reported that PWHT of this hardfacing deposits is recommended in high load test conditions, where the principal wear mechanism is not oxidative [22, 25]. In this sense, the identification of the actual wear mechanism is of strong importance to promote the microstructure which allows achieving the properties required to ensure the service life of a component. Additionally, the

samples welded both under a shielding gas with higher CO_2 content and with higher heat input (THP and TH) showed the highest wear rate. This may be explained by their microstructural features as these samples presented the highest carbide precipitation, during the welding process.

3.5.2. Worn surfaces and oxides

The damage produced on the worn surfaces during the test was analysed on cross sections of the tested specimens. In the area adjacent to the worn surface, plastic flow of material oriented parallel to the sliding direction was observed (Figure 15) as well as reoriented laths of martensite and retained austenite transformed into tempered martensite. The depth of the deformed zone was approximately 10 μm from the surface, as reported in previous papers [26-27].

Isolated oxide islands were found in all worn surfaces, as can be seen in Figure 16a. Figure 16b shows EDS performed on zone A (oxide presence was confirmed by the EDS study). Abrasion lines, with orientation parallel to the sliding direction, were seen on the worn surfaces. These lines were produced by the rubbing of hard zones of the wheel during sliding [28-31]. Typical appearance of oxidative wear [29, 32] was found for all the conditions tested.

In Figure 17, a top view of the worn surface of the RCP sample can be seen. Comparing RC and RCP specimens, an increase in the amount of oxidized surface was seen in the heat treated RCP sample, which was in accordance with its lower oxidation resistance and higher wear rate, mentioned before.

XRD analysis was conducted on worn surfaces of the wheel and on the RC plate specimen to identify the presence of oxides. Figure 18 shows the obtained patterns on both worn surfaces.

It was found that the austenite retained on the surface was totally transformed and that, furthermore, oxide of the Fe_2O_3 type partially covered the worn surface. Both factors (complete transformation and Fe_2O_3 oxide type) improved wear resistance [33-34]. The oxide layers were preferentially present in zones with high plastic deformation. Although the measured temperature raised only to 130 ºC, based on the theory of oxidative wear, the local temperature could have reached up to 300-400 ºC [27], at which oxides could have been generated.

Figure 19a shows the microstructure on a longitudinal section adjacent to the worn surface of the reference material (AISI 1020 wheel) corresponding to 5000 m travel distance that was representative of

all cases analyzed. The main wear mechanisms identified on this material were oxidation and to a lesser extend abrasion. A strong strain hardening was also detected, leading to a hardness increase from 250 to 440 HV on a thickness of 200 microns approximately from the surface, as shown in Figure 19b. This hardening gave to this material a stable support to generate the oxide layer.

3.5.3. Debris

Figure 20a shows SEM images of debris collected for 3320 m of travel distance, corresponding to the RC specimens. The presence of oxides was determined through EDS (Figure 20b).

The particles observed in Figure 20a could be divided into two groups according to their sizes. Large particles of the order of one hundred microns with a plate shaped and debris morphology from the reference material and small particles of the order of ten microns from the hardfacing material (as determined with EDS, Figure 20b) were found. The large plate shaped particles and small debris were formed during the initial period during which wear was severe [30]. After some distance was covered, the surfaces oxidized and the material detached consisted in small oxide particles as shown in Figure 20. These small particles, generated in the stationary period, were mostly oxides with some small proportion of metallic particles. According to the literature [35], these oxides should show hardness values between 1000 and 2000 HV. Due to their high hardness these small particles could act as an abrasive element producing wear between both surfaces.

4. Conclusions

The change in the shielding gas showed a small effect on the weld deposit chemistry, with a small reduction in alloying content when the gas mixture employed was rich in CO_2. Welding with high heat input resulted in larger carbides precipitation, with increased darkening of the martensite phase due to the effect of successive passes, a reduction in the retained austenite content and lower hardness. The RC sample (welded with the lowest heat input and gas shielding with low CO_2 content) exhibited the highest alloy content, the highest proportions of retained austenite and highest hardness.

The post weld heat treatment resulted in a reduction of the Cr content in the matrix, with a reduction of 30% of resistance to oxidative wear under conditions of mild sliding and low load. This heat treatment, on

the other side, produced an increase in hardness due to secondary carbides precipitation. This shows the weak connection between hardness and wear resistance when the prevailing mechanism is oxidative wear. The shielding gas with high CO_2 content and the higher heat input, resulted in the least wear resistances due to Cr losses by carbides precipitation.

Due to the small change in wear resistance produced by variation in the shielding gas and heat input, it turns out advantageous to weld with high parameters, so the obtainment of the desired thickness of the overlay will be achieved with a smaller number of passes.

Acknowledgements

The authors wish to express their gratitude to EUTECTIC-CONARCO for supplying the consumable employed in this work and to ESAB Brazil for its manufacture, specific for this work; to AIR LIQUIDE Argentina for supplying the welding gases; to the INDUSTRIAL APPLICATIONS AREA of CONARCO-ESAB, Argentina for the facilities for the production of the welds; to ESAB Sweden for performing chemical analyses and to INTI (National Institute of Industrial Technology, Argentina, for the SEM work. Finally, the authors want to acknowledge to APUENFI, Argentina and to ANPCyT, Argentina for financial support.

References

[1] Merrick S, Kotecki D, Wu J. Materials and Applications - Part 2. 8 ed. Welding Handbook: American Welding Society; 1998.

[2] Huisman MD. Flux- and metal-cored wires, a productive alternative to stick electrodes and solid wires. Svetsaren 1996; 1-2: 6-14.

[3] Lyttle KA. Metal Cored Wires: Where Do They Fit in Your Future?. Welding Journal 1996; 75(10): 35-38.

[4] Myres D. Metal Cored Wires: Advantages and Disadvantages. Welding Journal 2002; 81(9): 39-42.

[5] Wu W, Hwu LY, Lin DY, Lee JL. The relationship between alloying elements and retained austenite in martensitic stainless steel welds. Scripta Materialia 2000; 42: 1071-1076.

[6] Koteki D, Ogborn J. Abrasion resistance of iron-based hardfacing alloys. Welding Journal 1995; 74 (8): 269s-278s.

[7] Avner H. Introducción a la Metalurgia Física 2ed: Mc Graw Hill; 1993.

[8] Bortoni OE, Patrone JJ, Marino P. Recargue por soldadura de superficies sometidas a desgaste. Siderurgia 1989; 49: 114-139.

[9] Vardavoulias M. The role of hard second phases in the mild oxidational wear mechanism of high-speed steel-based materials. Wear 1994; 173: 105-114.

[10] Beymon JH. Tribology of hot metal forming. Tribology International 1998; 3(1-3): 73-77.

[11] Lim SC. Recent development in wear-mechanism maps. Tribology International 1998; 31(1-3): 87-97.

[12] Cullity BD, Stock SR. Elements of X-ray diffraction. Prentice Hall ed; 2001.

[13] Kim C, Biss V, Hosford WF. A new procedure for determining volume fraction of primary carbides in high-speed and relate tool steels. Metallurgical Transactions A 1982; 13A(2): 185-191.

[14] Gualco A, Svoboda H, Surian E, Ramini M, De Vedia L. Dilution study in hardfacing deposits (in spanish). Sam-Conamet. 2005. Mar del Plata, Argentina.

[15] Vaidya V. Shielding gas mixtures for semiautmatic welds. Welding Journal 2002; 81(9): 43-48.

[16] Rissone M, Svoboda H, De Vedia L, Surian E. Influence of procedure variables on C-Mn-Ni-Mo metal cored wire ferritic all-weld metal. Welding Journal 2005; 10: 139-148.

[17] Kalousek J, Fegrego DM, Laufer EE. The wear resistance and worn metallography of pearlite, bainite and tempered martensite rail steel microstructures of high hardness. Wear 1985; 105(3): 199-222.

[18] Leshchinskiy LK, Samotugin SS. Mechanical properties of plasma-hardened 5% chromium tool steel deposited by arc welding. Welding Journal 2001; 80(1): 25-30.

[19] Verhoeven JD. Fundamentos de Metalurgia Física. 1 ed: Limusa; 1987.

[20] Dobrzanski LA, Mazurkiewicz J, Hajduczek E. Effect of thermal treatment on structure of newly developed 47CrMoWVTiCeZr16-26-8 hot-work tool steel. Journal of Materials Processing Technology 2004; 157-158: 472-484.

[21] Dumovic M. Repair and maintenance procedures for heavy-machinery components. Welding Innovation 2003; XX(1): 1-5.

[22] Gualco A, Svoboda H, Surian E, De Vedia L. Effect of post-weld heat treatment on wear resistance of martensitic steel harfacing deposits. Soldagem & Inspeçao 2008; 13(3): 237-244.

[23] Eyre TS, Maynard D. Surface aspects of unlubricated metal-to-metal wear. Wear 1971; 18(4): 301-310.

[24] Cui XH, Wang SQ, Wang F,Chen KM. Research on oxidation wear mechanism of the cast steels. Wear 2008; 265: 468-476.

[25] Gualco A, Svoboda H, Surian E, De Vedia L. Effect of welding procedure on severe wear resistance of martensitic hardfacing deposits. I CAIM 2008: UTN-Bahía Blanca, Argentina.

[26] Hurricks PL. Some aspects of the metallurgy and wear resistance of surface coatings. Wear 1972; 22(3): 291-320.

[27] Hogmark S, Vingsbo O, Fridström S. Mechanisms of dry wear of some martensitic steels. Wear 1975; 31: 39-61.

[28] Fontalvo GA, Mitterer C. The effect of oxide-forming alloying elements on the high temperature wear of a hot work steel. Wear 2005; 258: 1491-1499.

[29] Quinn TFJ, Sullivan JL, Rowson DM. Origins and development of oxidational wear at low ambient temperatures. Wear 1984; 94: 175-191.

[30] Bahrami A, Anijdan SHM, Golozar MA, Shamanian M, Varahram N. Effects of conventional heat treatment on wear resistance of AISI H13 tool steel. Wear 2005; 258: 846-851.

[31] Wang Y, Lei T, Liu J. Tribo-metallographic behavior of high carbon steels in dry sliding II. Microstructure and wear. Wear 1999; 231: 12-19.

[32] So H. The mechanism of oxidational wear. Wear 1994; 184: 161-167.

[33] So H, Yu DS, Chuang CY. Formation and wear mechanism of tribo-oxides and the regime of oxidational wear of steel. 2002; 253: 1004-1015.

[34] Colaço R, Vilar R. On the influence of retained austenite in the abrasive wear behaviour of a laser surface melted tool steel. Wear 2005; 258: 225-231.

[35] Barrau O, Boher C, Vergne C, Rezai-Aria F. Investigations of friction and wear mechanisms of hot forging tool steels. Proceedings of the 6th International Tooling Conference; 2002.

Captions of Tables and Figures

Table 1

Sample identification	Shielding gas	Heat input (kJ/mm)	Arc voltage (V)	Welding current (A)	Welding speed (mm/s)	Oscillation (mm)
RC	Ar-2%CO_2	1.9	28	180	2.6	6
RH	Ar-2%CO_2	2.9	31	250	2.7	5
TC	Ar-20%CO_2	2.0	28	190	2.6	6
TH	Ar-20%CO_2	2.9	31	260	2.8	5

Table 2

Identification	C	Mn	Si	Cr	Mo	V	W	Shielding gas	Heat input (kJ/mm)
RC	0.48	1.30	0.67	5.5	2.6	0.40	1.9	Ar-2%CO_2	1.9
RH	0.44	1.20	0.60	5.3	2.4	0.34	1.8	Ar-2%CO_2	2.9
TC	0.40	1.20	0.49	5.5	2.4	0.34	1.9	Ar-20%CO_2	2.0
TH	0.47	1.10	0.49	5.3	2.3	0.36	1.8	Ar-20%CO_2	2.9

Figure 1

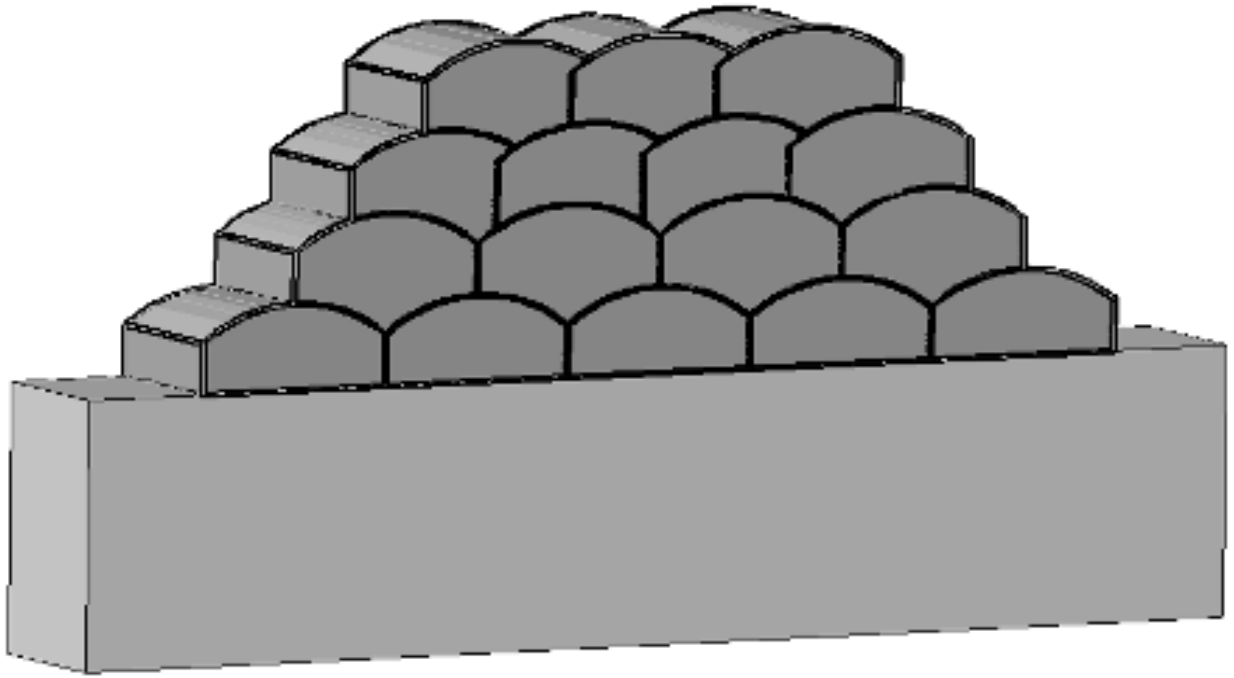

Figure 2

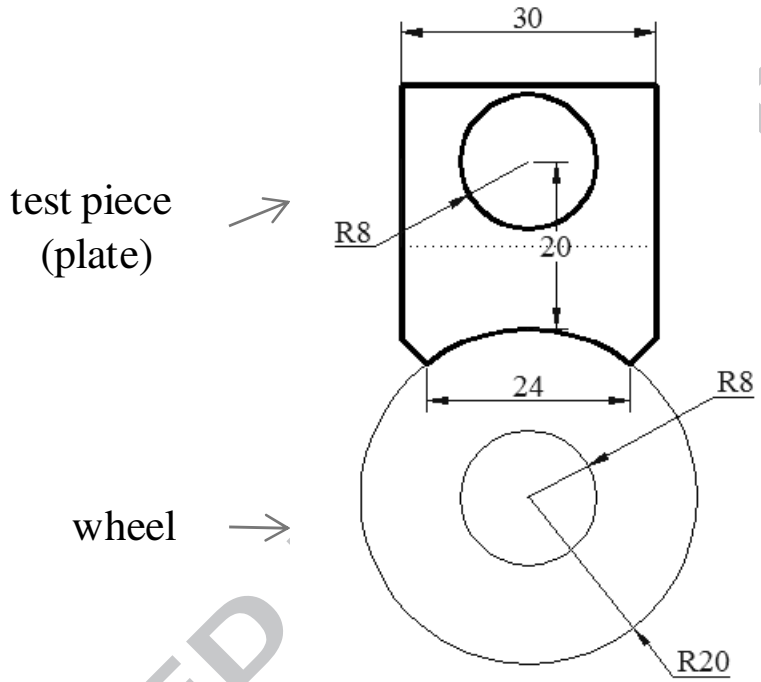

Figure 3

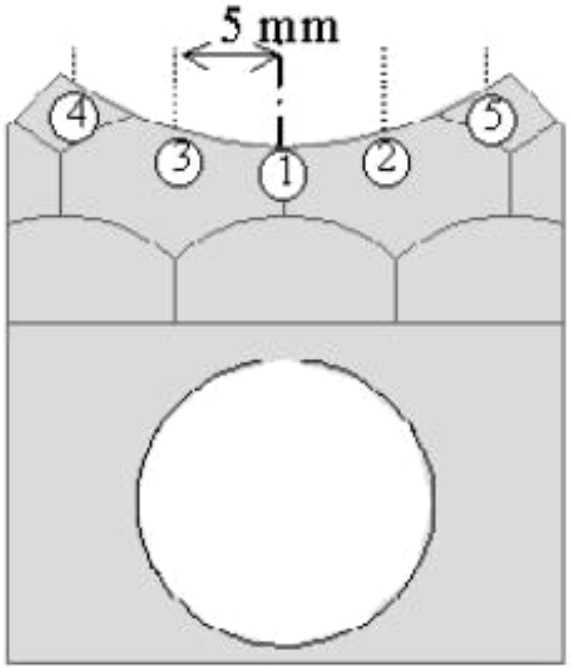

Figure 4

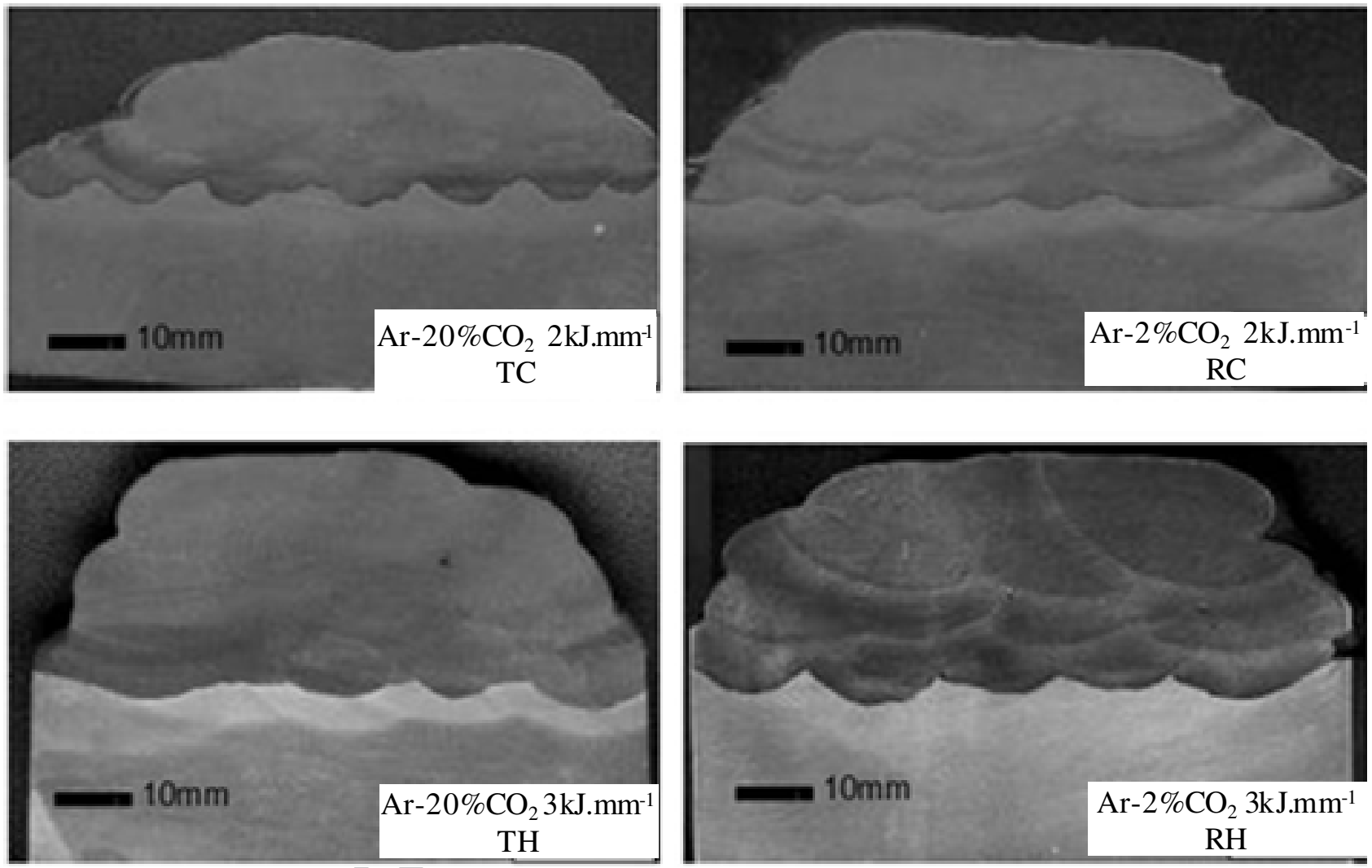

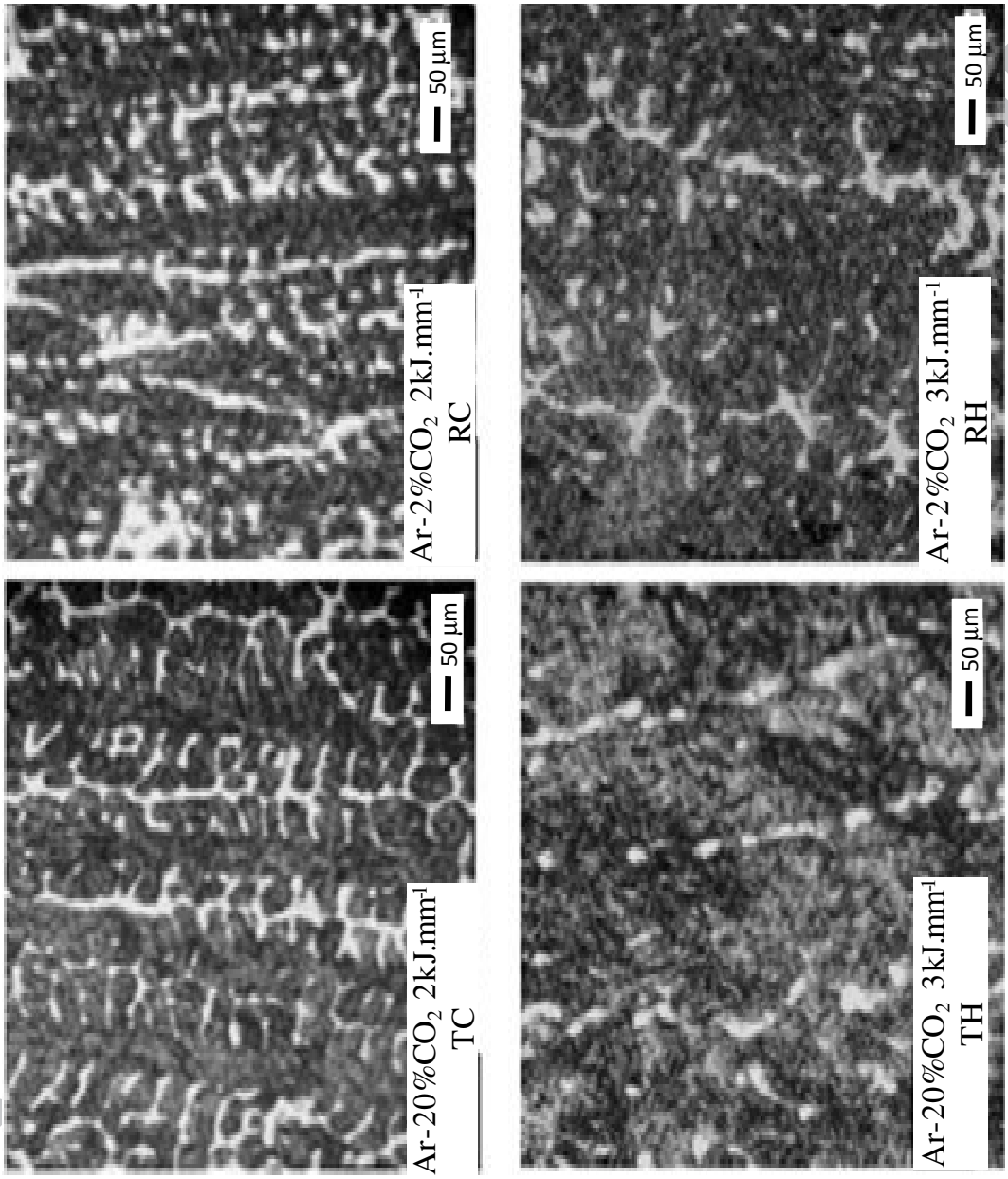

Figure 5

Figure 6

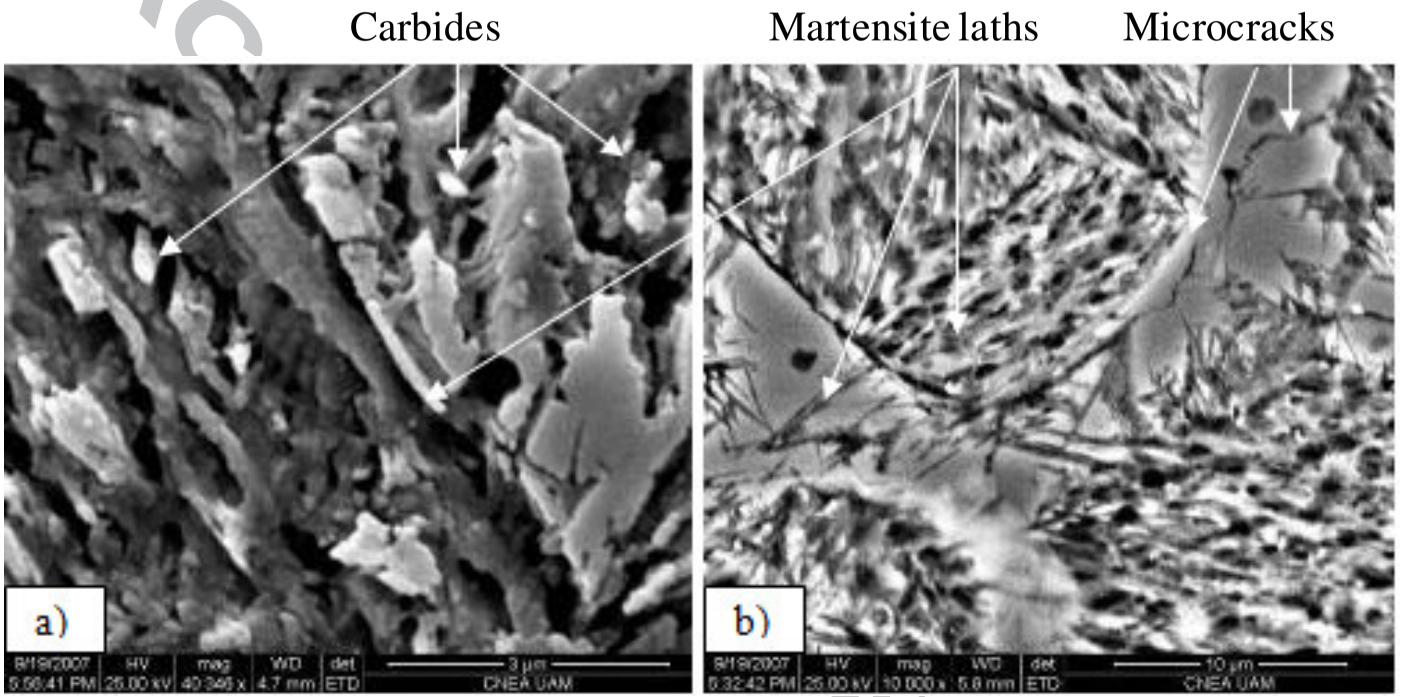

Figure 7

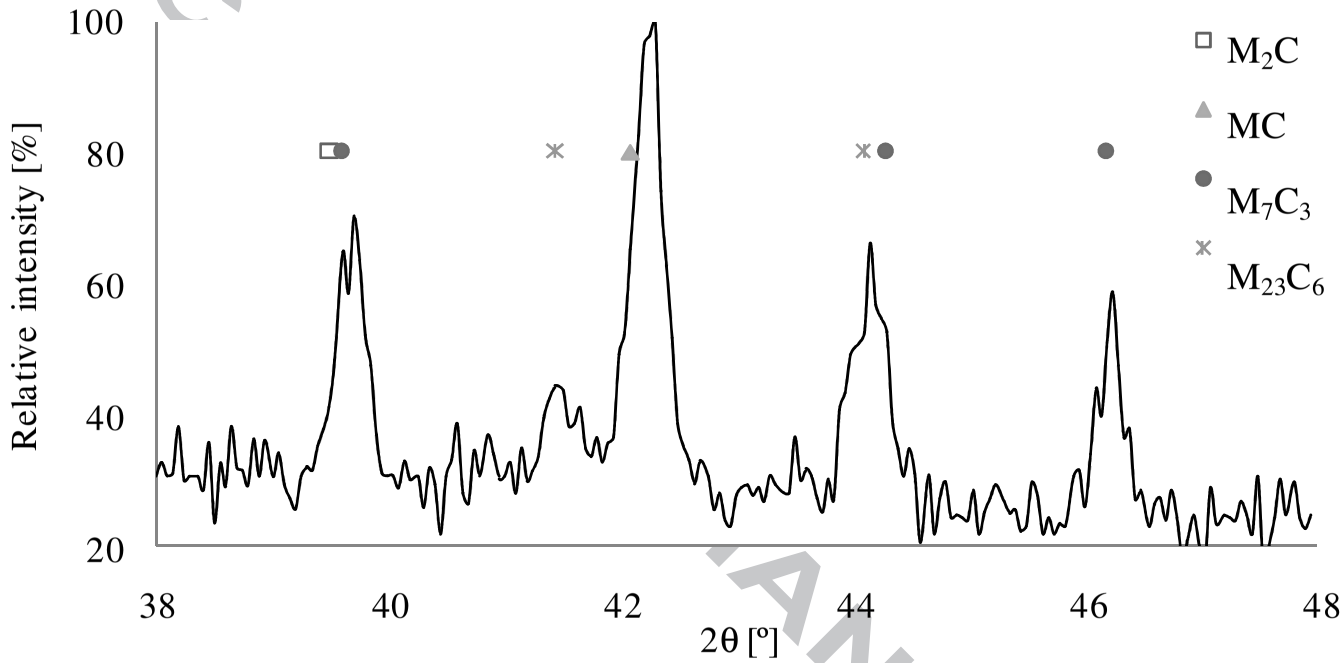

Figure 8

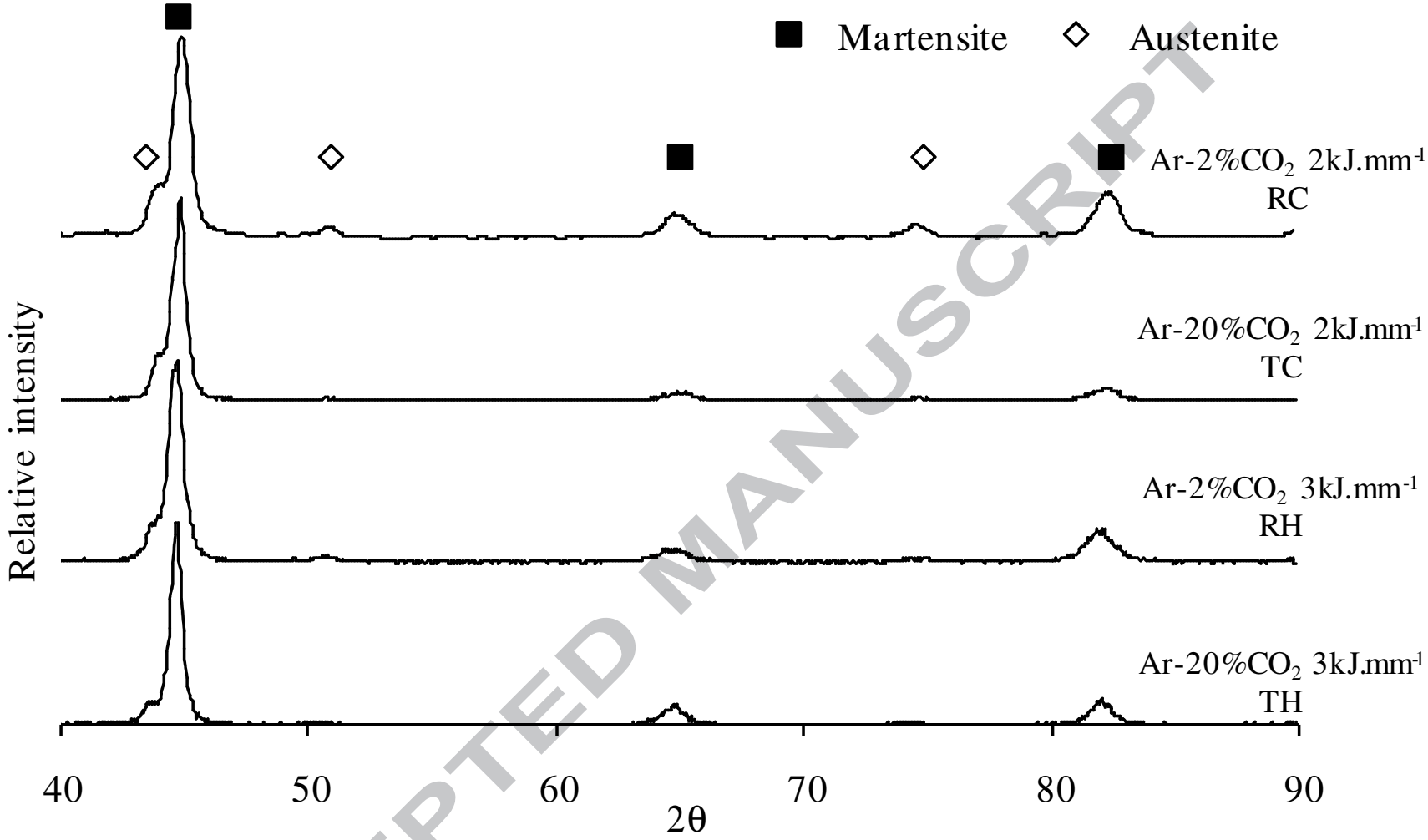

Figure 9

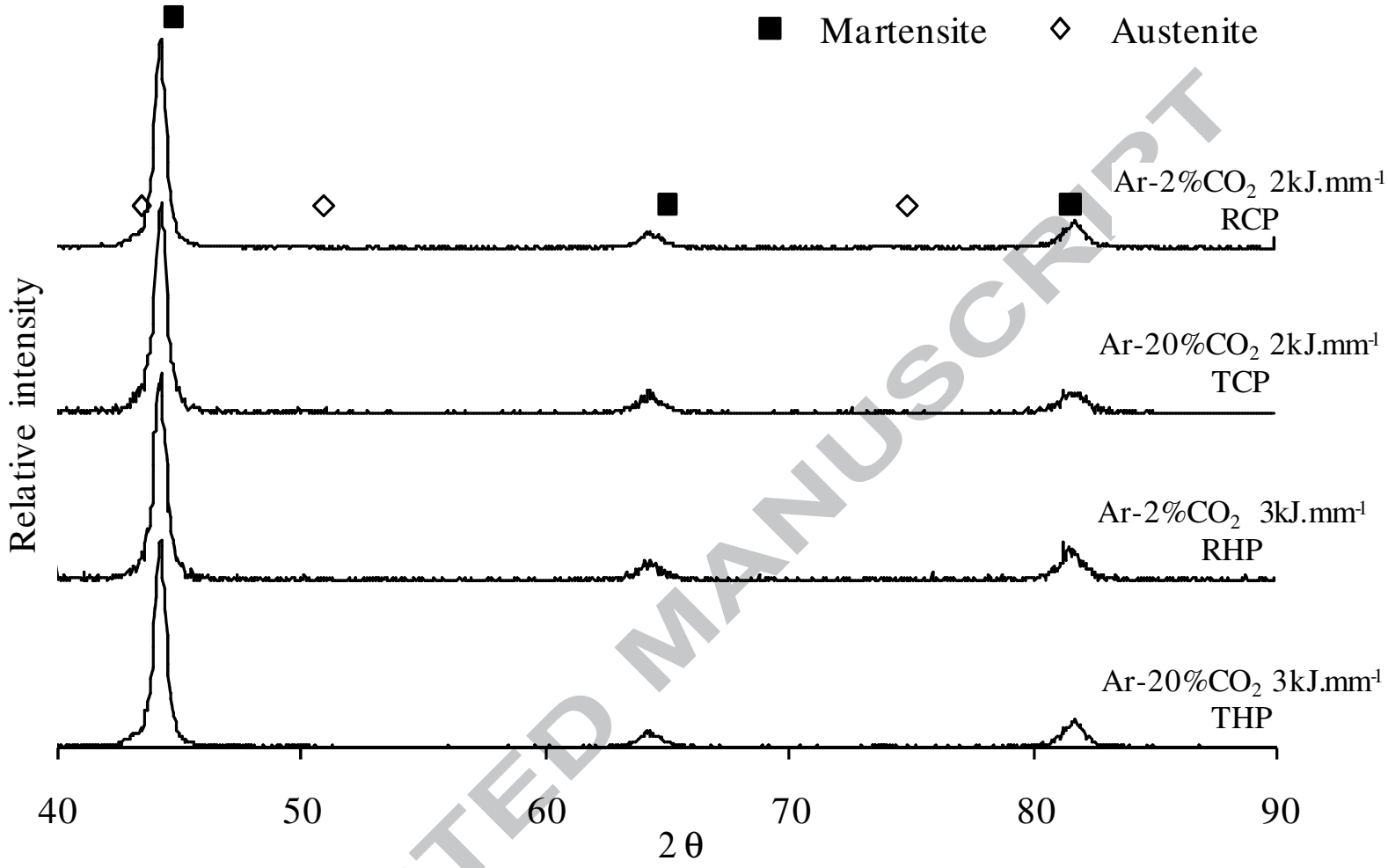

Figure 10

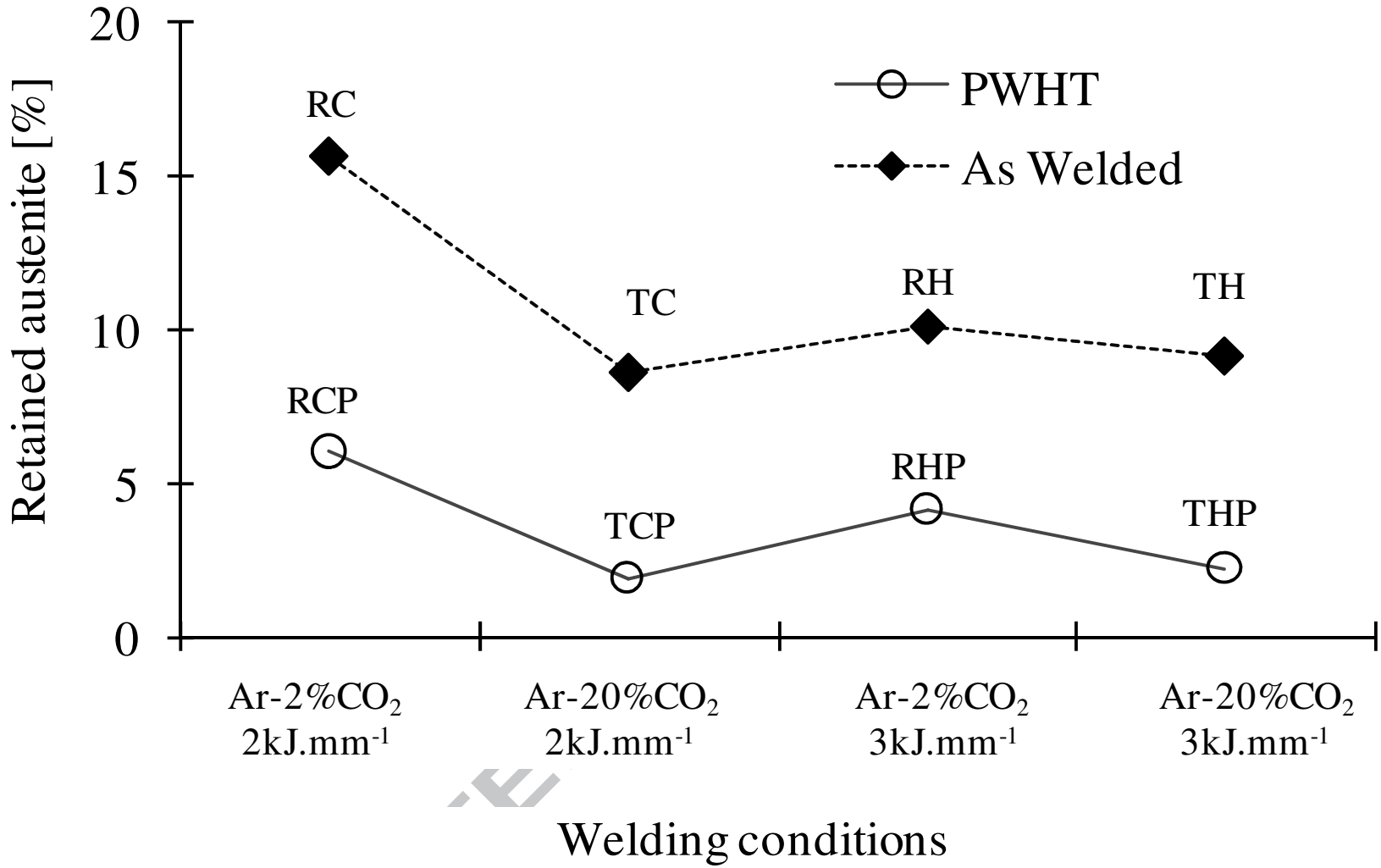

Figure 11

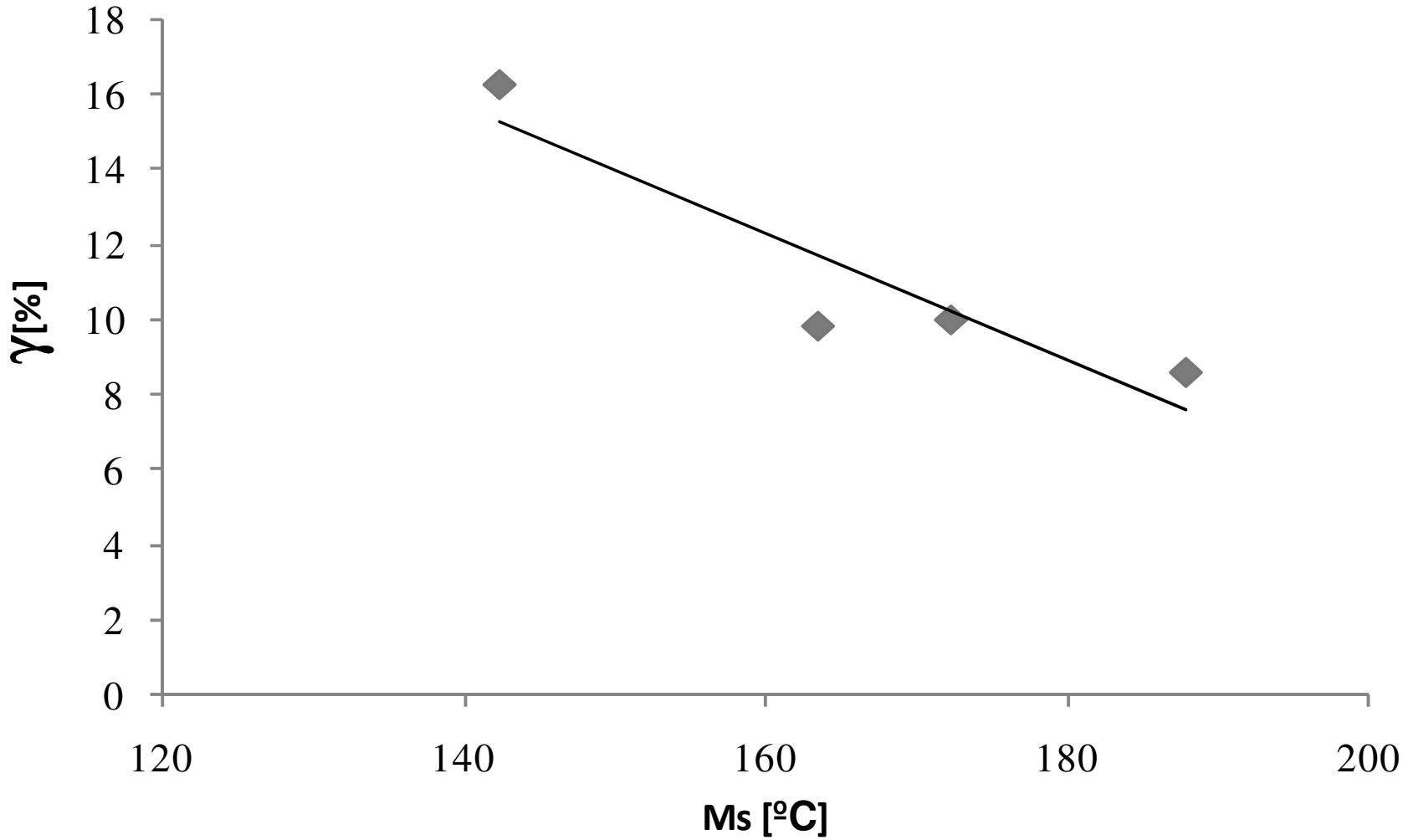

Figure 12

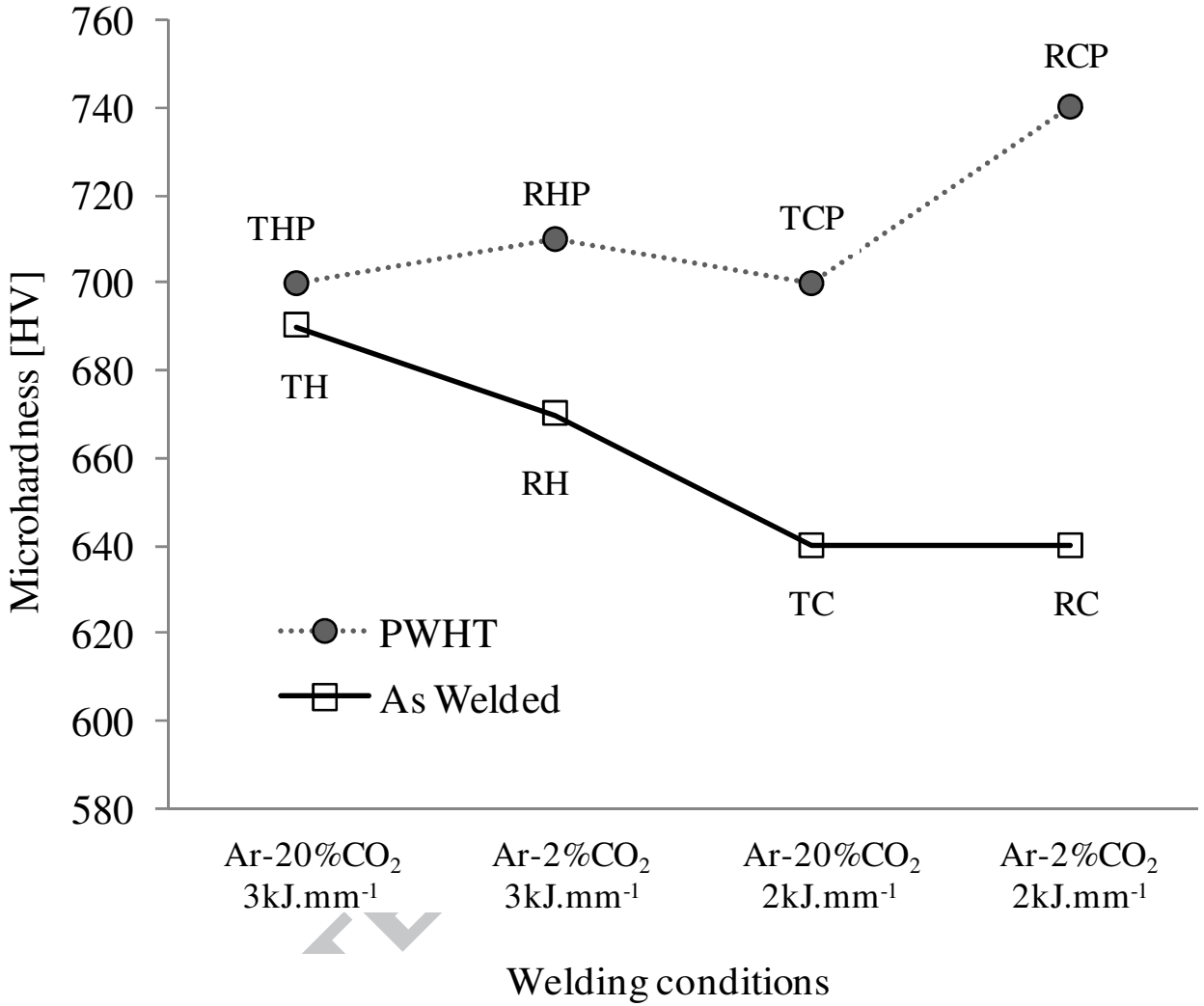

Figure 13

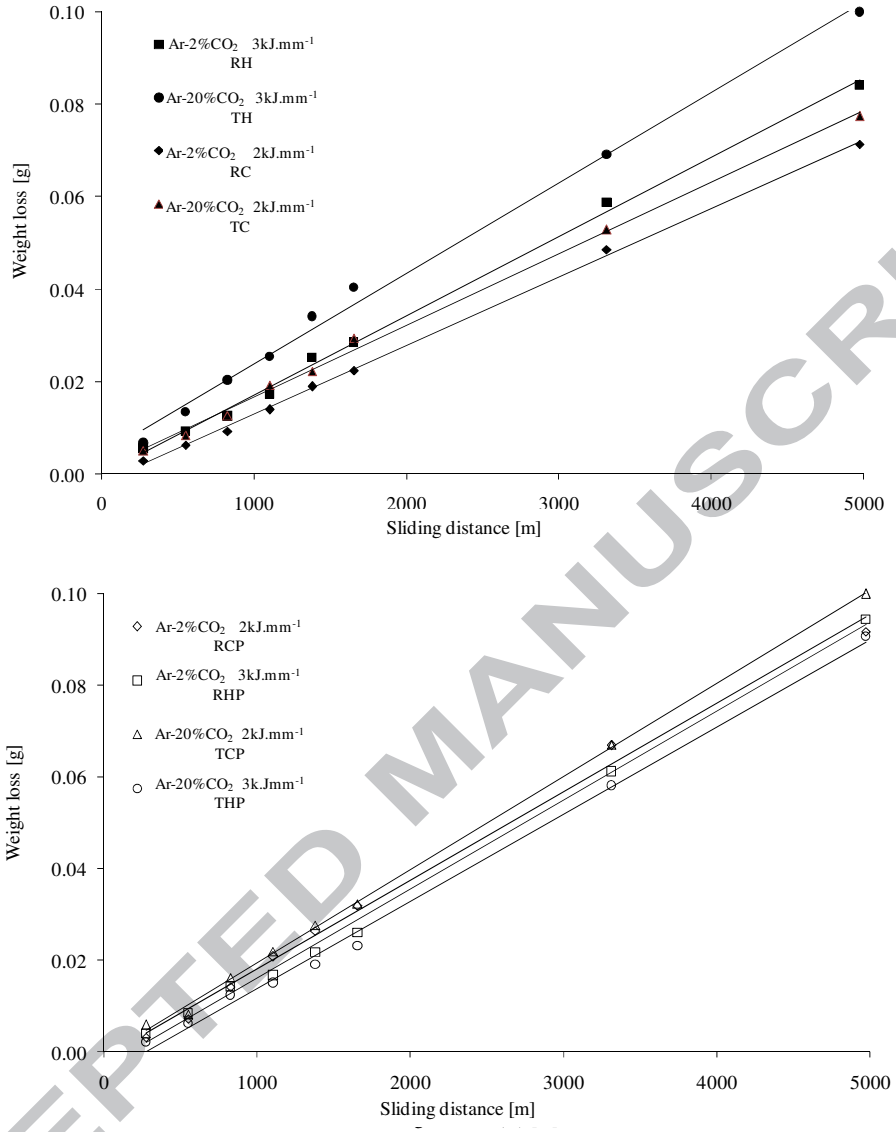

Figure 14

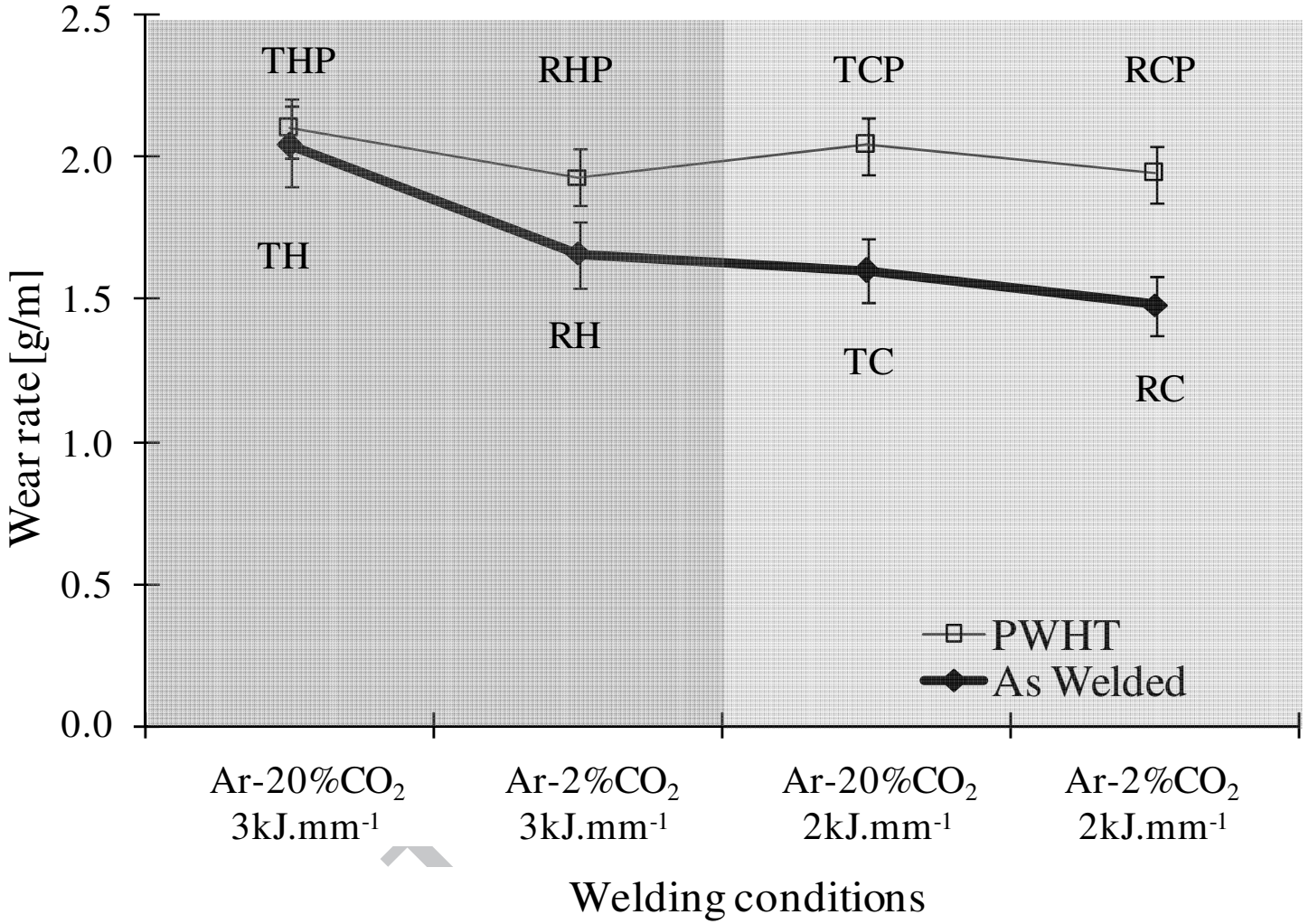

Figure 15

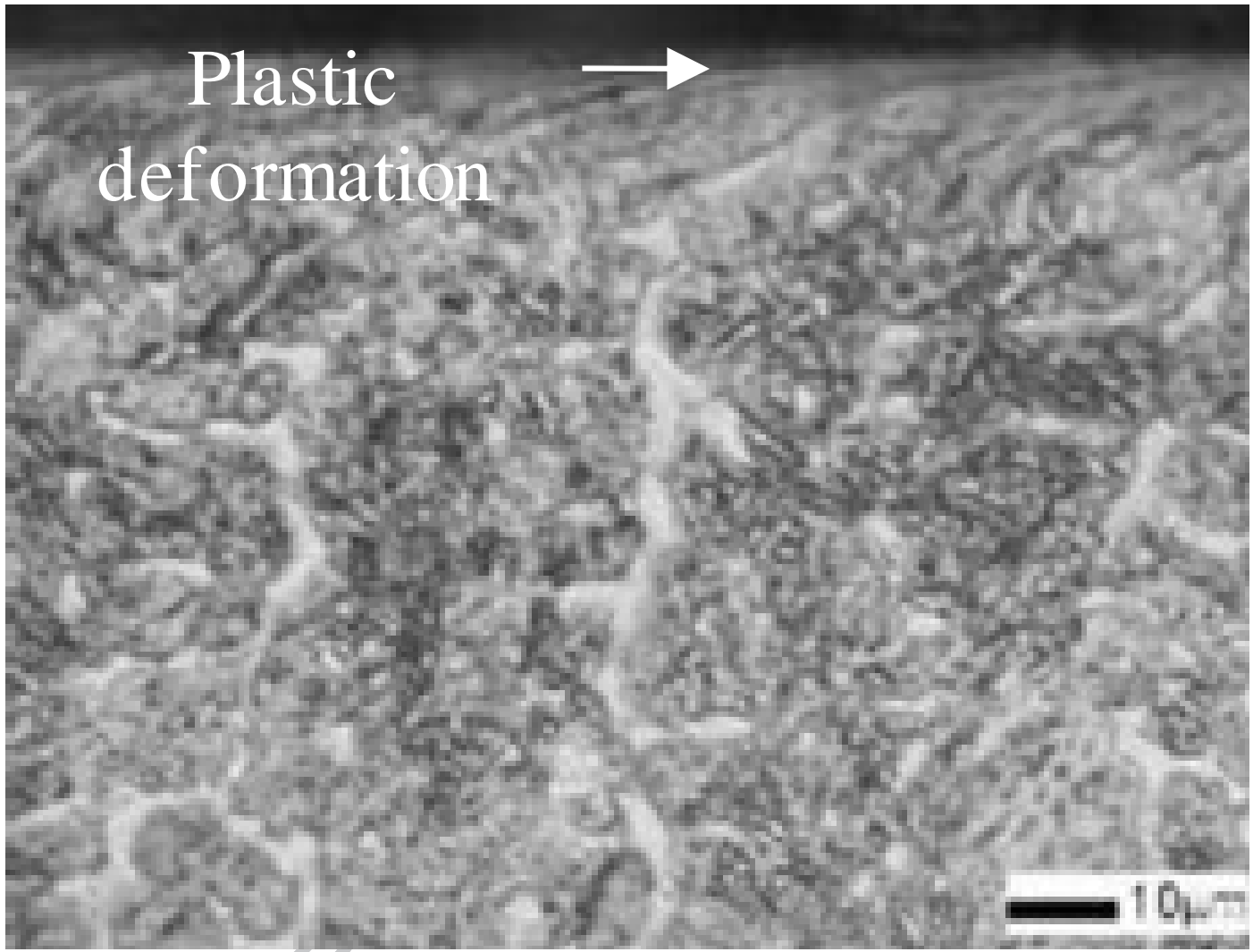

Figure 16a

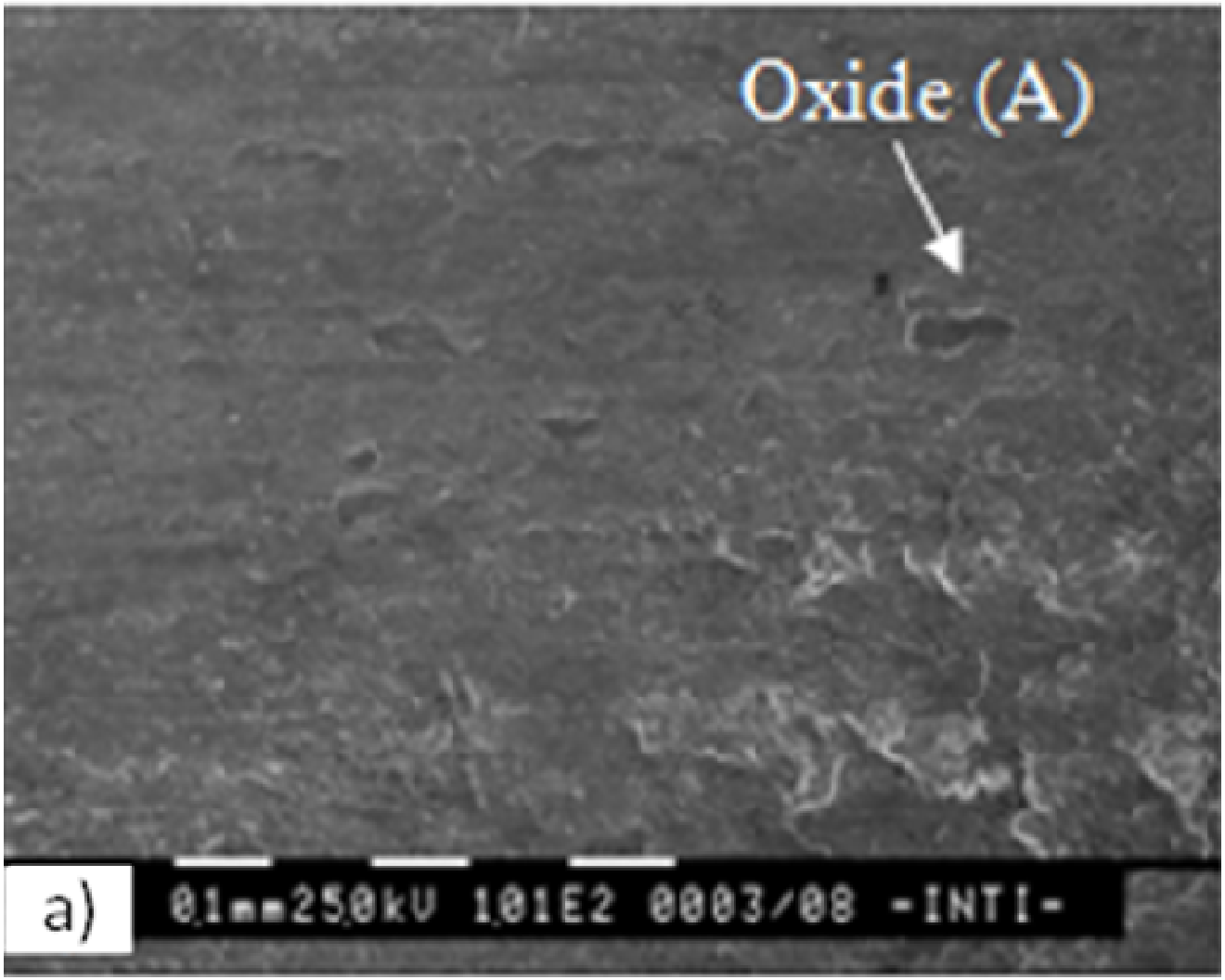

Figure 16b

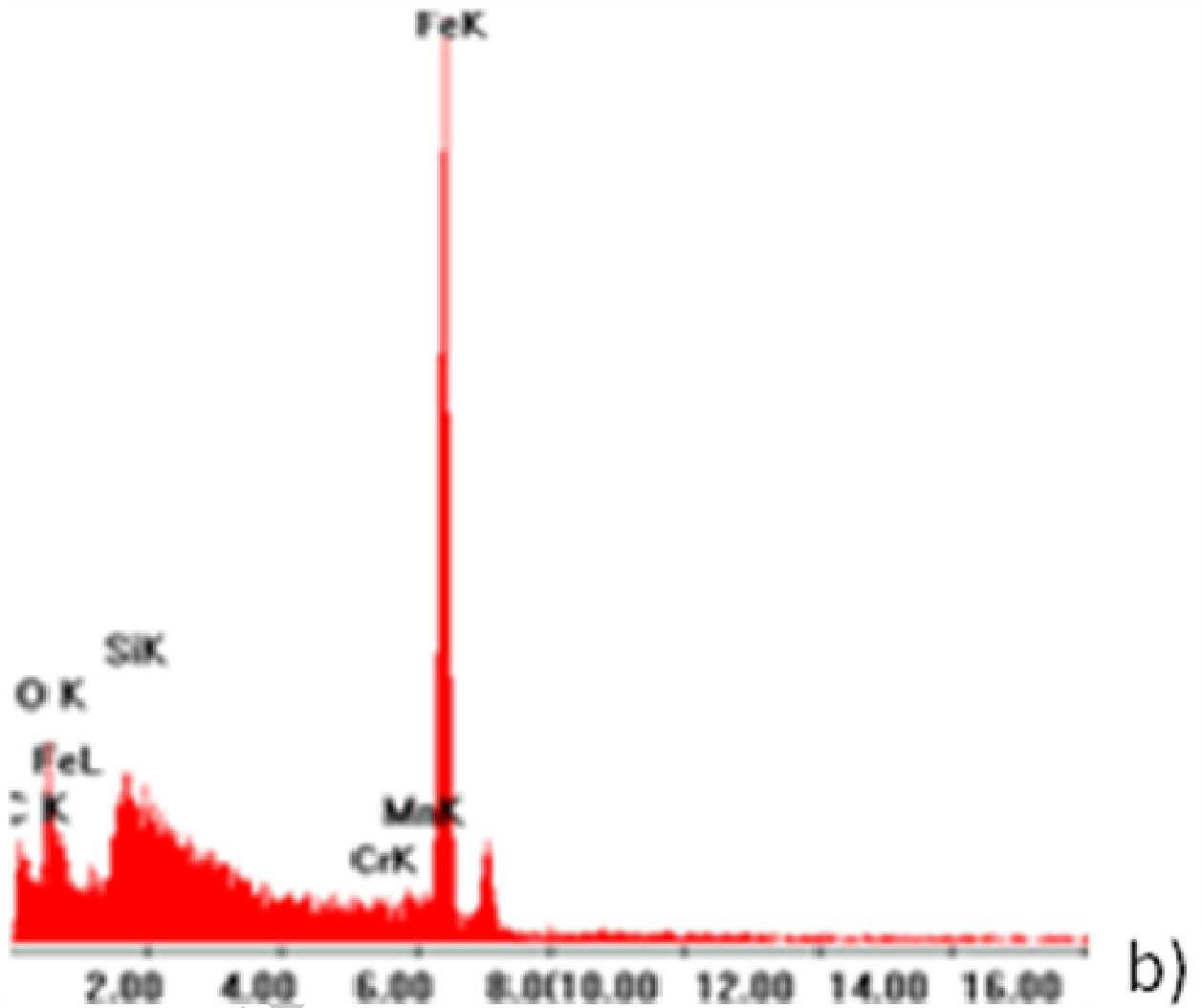

Figure 17

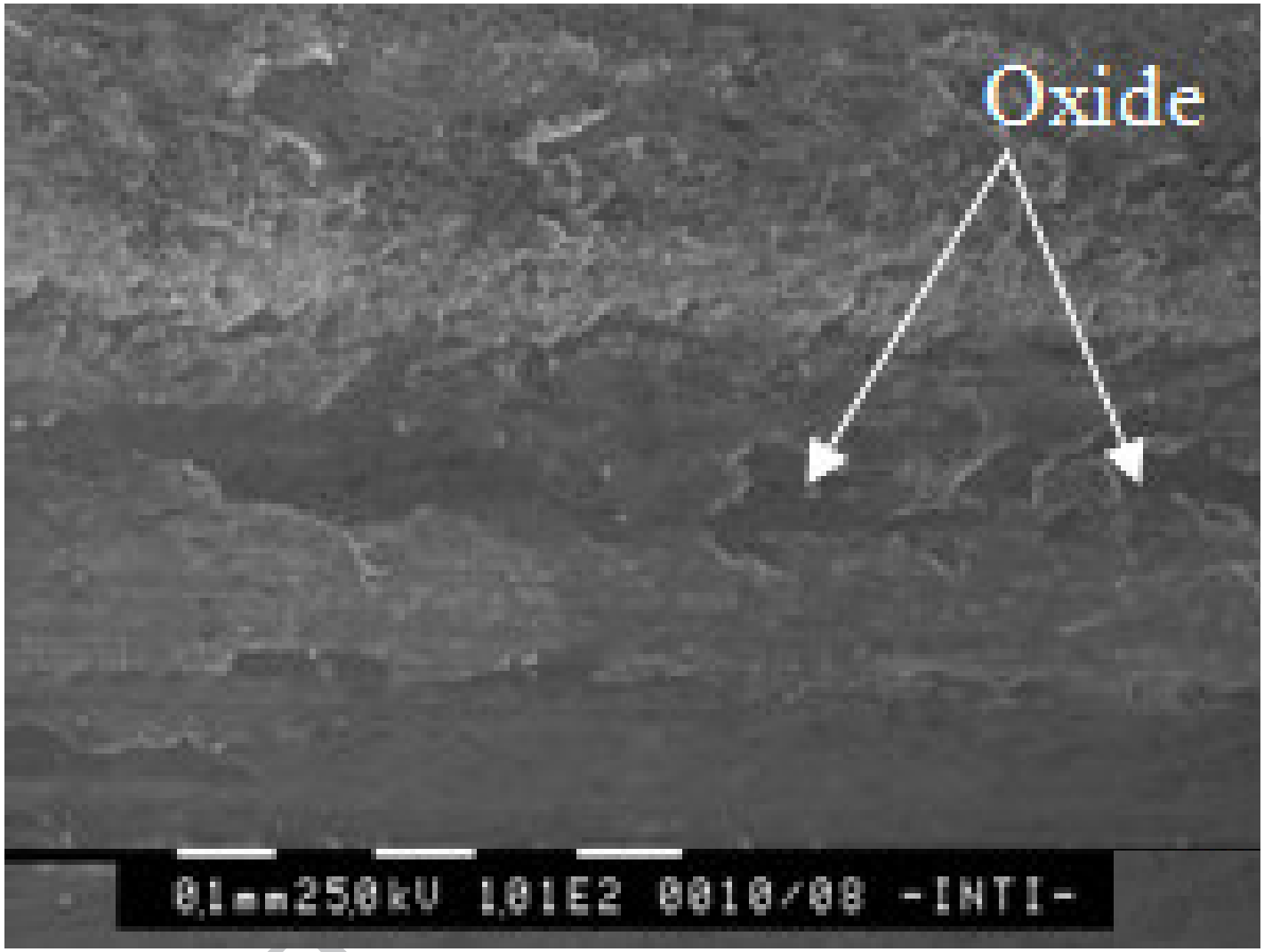

Figure 18

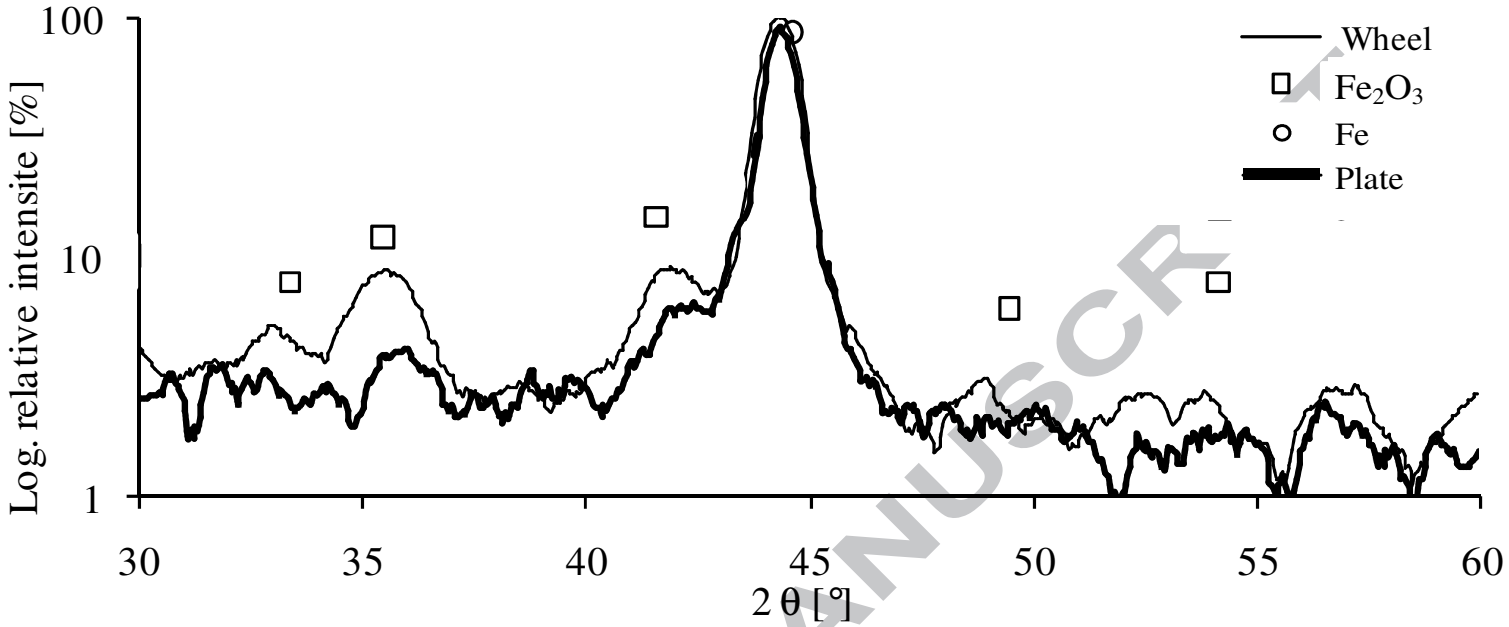

Figure19a

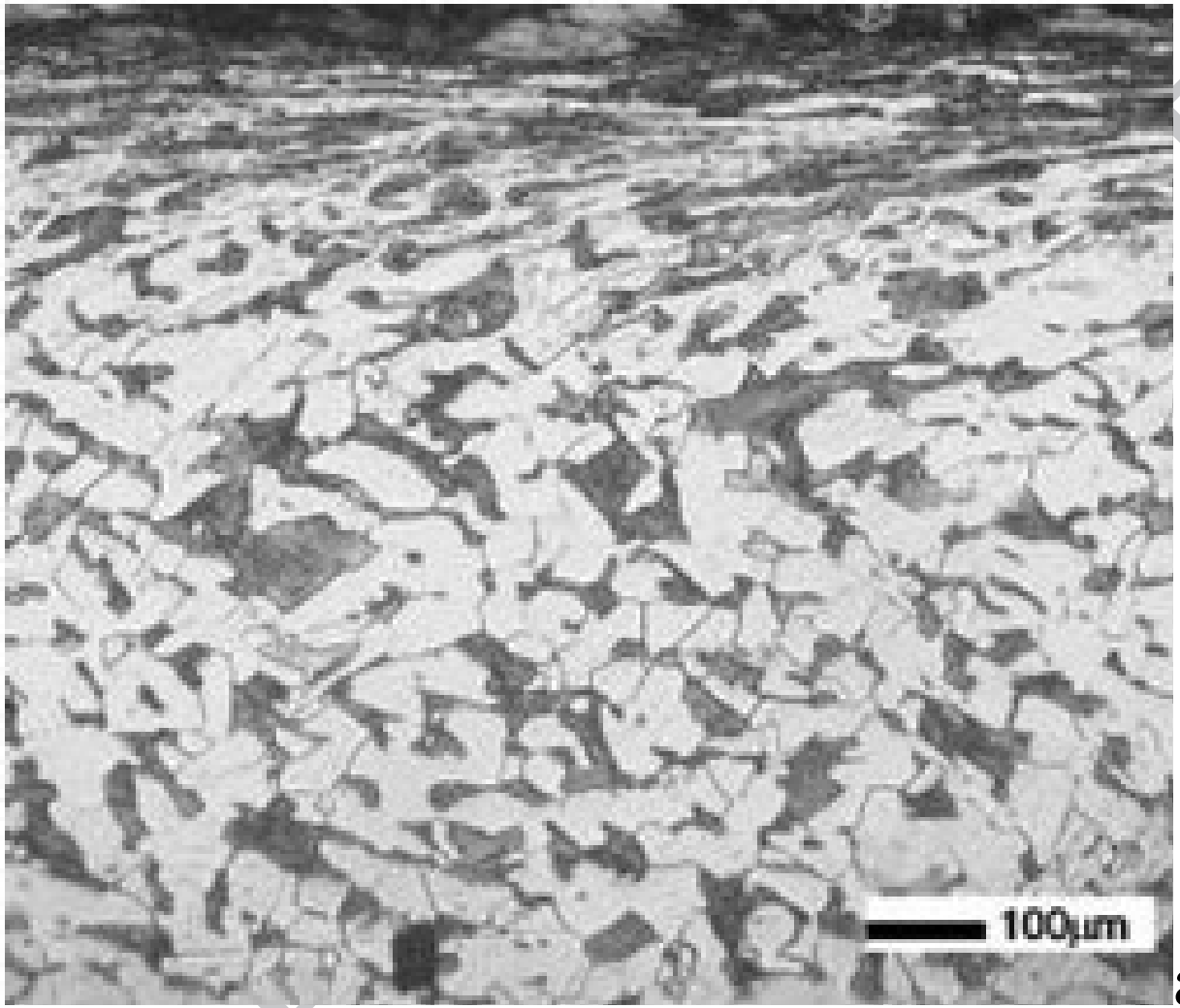

a)

Figure19b

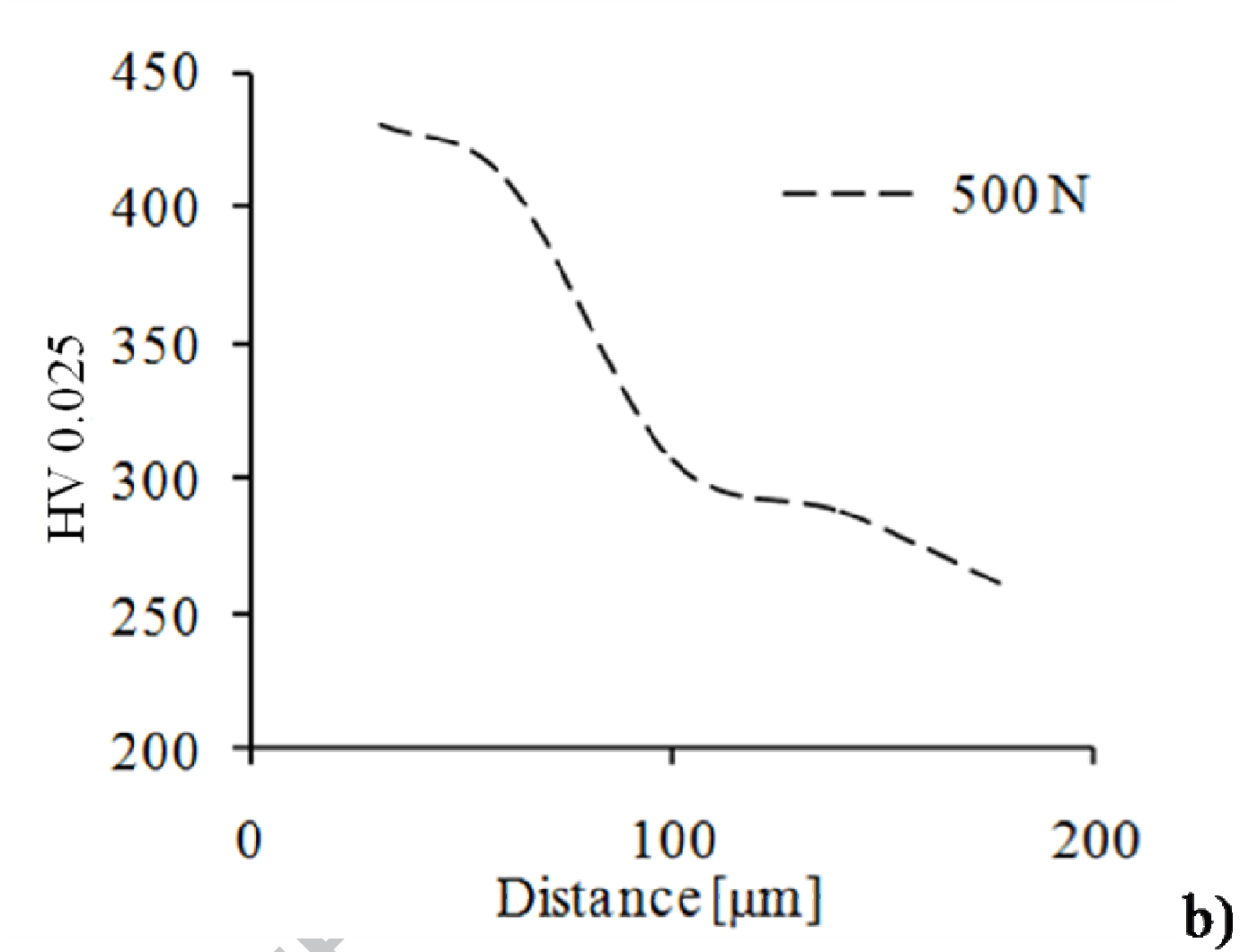

Figure 20a

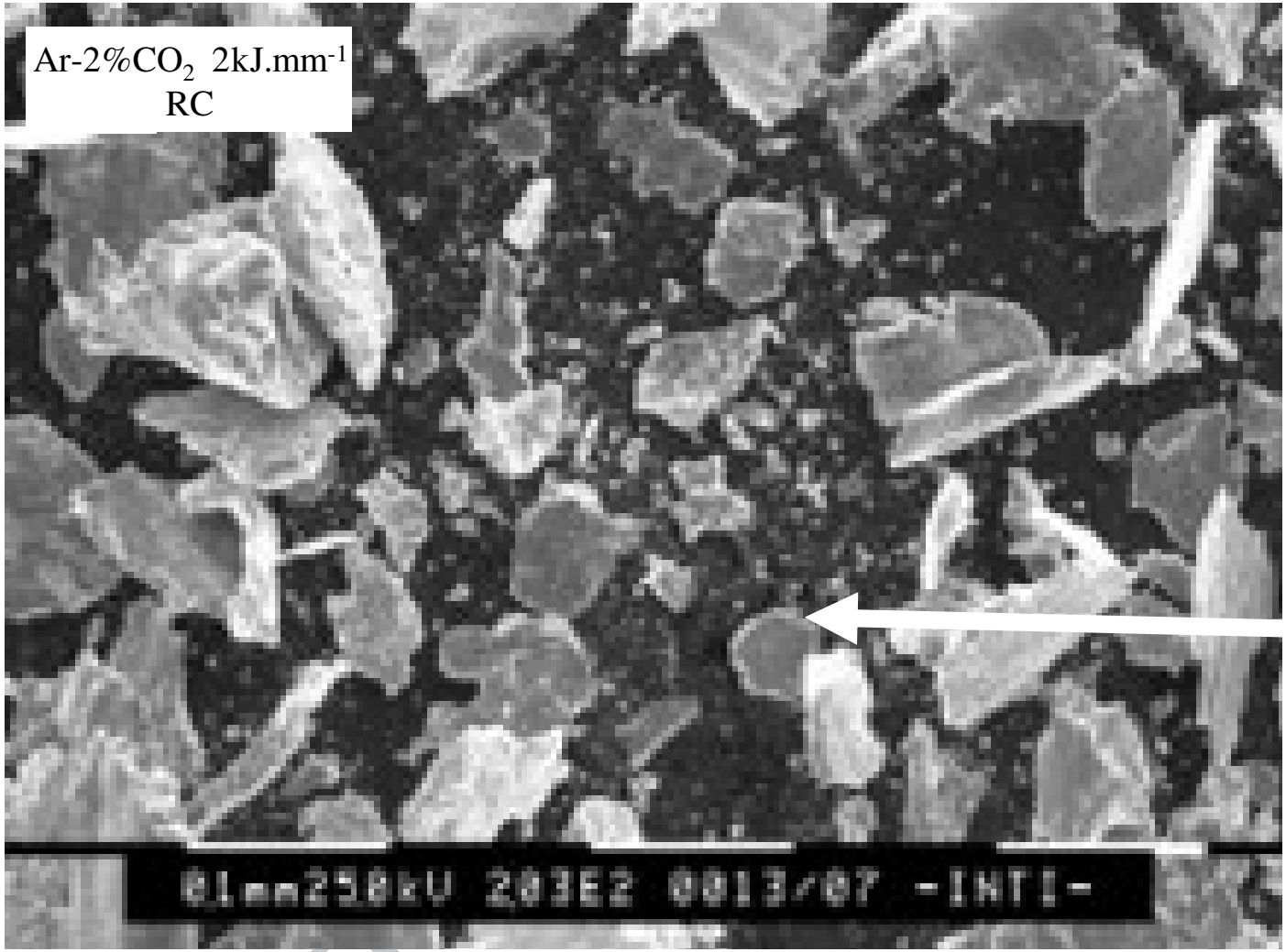

a)

Figure 20b

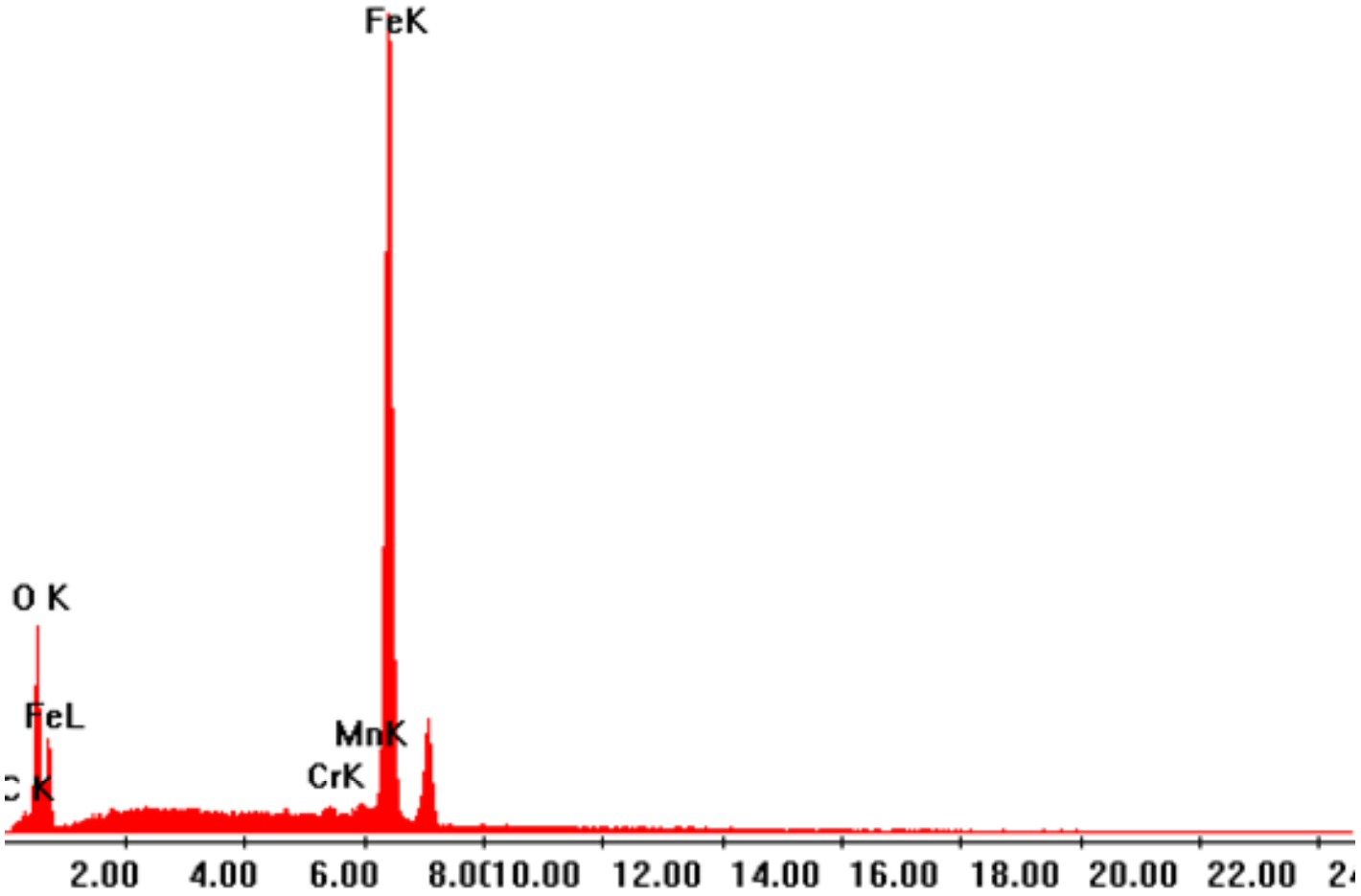

b)